

## Elliptic flow in Au+Au collisions at $\sqrt{s_{NN}} = 130$ GeV

R.J.M. Snellings<sup>a</sup> for the STAR collaboration\*

<sup>a</sup>Lawrence Berkeley National Laboratory,  
1 Cyclotron Road, Berkeley, California 94720, United States

We report the elliptic flow of charged and identified particles at mid-rapidity in Au+Au collisions at  $\sqrt{s_{NN}} = 130$  GeV using the STAR TPC at RHIC. The integrated elliptic flow signal,  $v_2$ , for charged particles reaches values of about 0.06, indicating a higher degree of thermalization than at lower energies. The differential elliptic flow signal,  $v_2(p_t)$  up to 1.5 GeV/c, shows a behavior expected from hydrodynamic model calculations. Above 1.5 GeV/c, the data deviate from the hydro predictions; however the  $v_2(p_t)$  is still large, suggesting finite asymmetry for the products of hard scattering. For the identified particles, elliptic flow as a function of  $p_t$  and centrality differ significantly for particles of different masses. This dependence can be accounted for in hydrodynamic models, indicating that the system created shows a behavior consistent with collective hydrodynamical flow.

### 1. Introduction

The goal of the ultra-relativistic nuclear collision program is the creation of a system of deconfined quarks and gluons [1]. The azimuthal anisotropy of the transverse momentum distribution for non-central collisions is thought to be sensitive to the early evolution of the system. The second Fourier coefficient of this anisotropy,  $v_2$ , is called elliptic flow. It is an important observable since it is sensitive to the rescattering of the constituents in the created hot and dense matter. This rescattering converts the initial spatial anisotropy, due to the almond shape of the overlap region of non-central collisions, into momentum anisotropy. The spatial anisotropy is largest early in the evolution of the collision, but as the system expands and becomes more spherical, this driving force quenches itself. Therefore, the magnitude of the observed elliptic flow reflects the extent of the rescattering at early time [2].

Elliptic flow in ultra-relativistic nuclear collisions was first discussed in Ref. [3] and has been studied intensively in recent years at AGS [4,5], SPS [6–8] and RHIC [9] energies. The studies at the top AGS energy and at SPS energies have found that elliptic flow at these energies is in the plane defined by the beam direction and the impact parameter,  $v_2 > 0$ , as expected from most models.

The Solenoidal Tracker At RHIC (STAR) [10] measures charged particles, and due to its azimuthal symmetry and large coverage, it is ideally suited for measuring elliptic flow. The detector consists of several sub-systems in a large solenoidal magnet. The Time Projection Chamber (TPC) covers the pseudorapidity range  $|\eta| < 1.8$  for collisions in the

---

\*For complete author list see J.W. Harris, these proceedings

center of the TPC. The magnet is operated at a 0.25 Tesla field, allowing tracking of particles with  $p_t > 75$  MeV/c. Two Zero Degree Calorimeters [11] located at  $\theta < 2$  mrad, which mainly detect fragmentation neutrons, are used in coincidence for the trigger. The TPC is surrounded by a scintillator barrel which measures the charged particle multiplicity for triggering purposes within  $|\eta| < 1$ .

For this analysis, 120,000 events were selected with a primary vertex position within 75 cm longitudinally of the TPC center and within 1 cm radially of the beam line. For determination of the event plane, charged particle tracks were selected with  $0.1 < p_t \leq 2.0$  GeV/c. The tracks used to determine the event plane and the tracks correlated with the event plane passed within 2 cm of the primary vertex and had at least 15 measured space points. Also, the ratio of the number of space points to the expected maximum number of space points for that particular track was required to be greater than 0.52, suppressing split tracks from being counted more than once. The tracks used for the determination of the reaction plane were within  $|\eta| < 1.0$ , and the tracks correlated with the reaction plane were within  $|\eta| < 1.3$ . These cuts are similar to the ones used in Ref. [9] where it was shown that the analysis results are not sensitive to the cuts.

## 2. Charged-particle elliptic flow

The flow analysis method [12] involves the calculation of the event plane angle, which is an experimental estimator of the real reaction-plane angle. The second harmonic

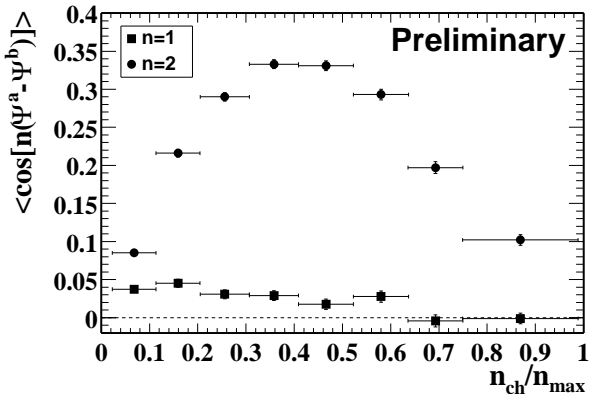


Figure 1. The correlation between the event plane angles determined for two independent sub-events. The correlation is calculated for the first harmonic ( $n=1$ ) and the second harmonic ( $n=2$ ).

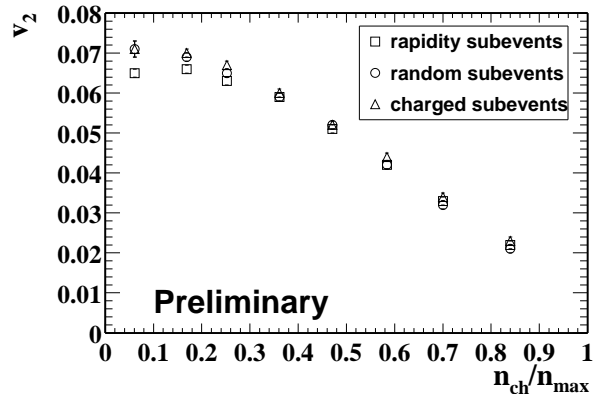


Figure 2. The integrated elliptic flow signal,  $v_2$ , determined using three different sub-event methods.

event plane angle,  $\Psi_2$ , is calculated for two sub-events, which are independent subsets of all tracks in each event. Figure 1 shows the results for the correlation between the sub-events for the first and second harmonic as a function of centrality [9]. The peaked shape of the centrality dependence of  $\langle \cos[2(\Psi_a - \Psi_b)] \rangle$  is a signature of anisotropic flow. However, the correlation between the sub-events may not be due entirely to anisotropic

flow. To estimate the magnitude of non-flow effects we have chosen the sub-events in three different ways: 1) Assigning particles with pseudorapidity  $-1 < \eta < -0.05$  to one sub-event and particles with  $0.05 < \eta < 1$  to the other. Short range correlations, such as Bose-Einstein or Coulomb, are to a large extent eliminated by the “gap” between the two sub-events. 2) Dividing randomly all particles into two sub-events, sensitive to all non-flow effects. 3) Assigning positive particles to one sub-event and negative particles to the other, allowing an estimation of the contribution from resonance decays. In Fig. 2 the resulting  $v_2$  versus centrality from each of these methods is shown. The charged particles were integrated over  $0.1 < p_t < 2.0$  GeV/ $c$  and  $|\eta| < 1.3$ . The results from the three methods are for the central and mid-peripheral events very similar. However, for the most peripheral events the results vary among the methods by about 0.005.

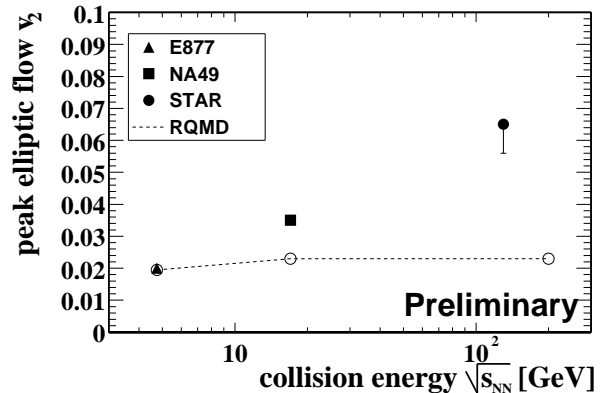
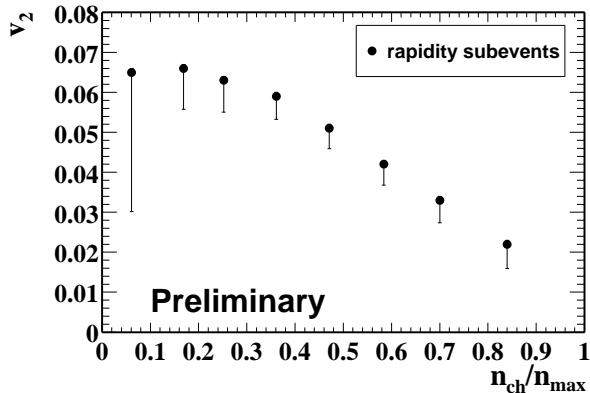


Figure 3. The integrated elliptic flow signal,  $v_2$ , with the estimated systematic uncertainties.

Figure 4. Excitation function of  $v_2$  from top AGS to RHIC energies.

Not all non-flow contributions might be known and the effects of others, such as jets, are difficult to estimate because of their long-range correlation. Recently new methods to estimate these non-flow effects have become available [13]. In order to estimate the systematic uncertainty due to the effects of jets in this analysis, we assume that jets contribute at the same level to both the first and second order correlations. This assumption is verified by the Hijing [15] model. Taking the maximum observed positive first order correlation, 0.05, as being completely due to non-flow will reduce the calculated  $v_2$  values. Figure 3 shows  $v_2$  versus centrality, where the statistical uncertainties are smaller than the markers and the uncertainties shown are the systematic uncertainties due to this estimated non-flow effect.

Figure 4 shows the maximum  $v_2$  value as a function of collision energy. It rises monotonically from about 0.02 at the top AGS energy [4], 0.035 at the SPS [7] to about 0.06 at RHIC energies [9]. This increasing magnitude of the integrated elliptic flow indicates that the degree of thermalization, which is associated with the amount of rescattering, is higher at the higher beam energies. However, interpretation of the excitation function has to be done with care. The  $v_2$  values used here are the maximum values as a function of centrality for each energy. The centrality where  $v_2$  peaks can change as a function of

beam energy, indicating different physics [14].

### 2.1. Differential elliptic flow

The differential elliptic flow is a function of particle mass,  $\eta$  and  $p_t$ . Within  $|\eta| < 1.3$ ,  $v_2$  is approximately constant. In this section the  $v_2(p_t)$  will be discussed, the next section will discuss the mass dependence.

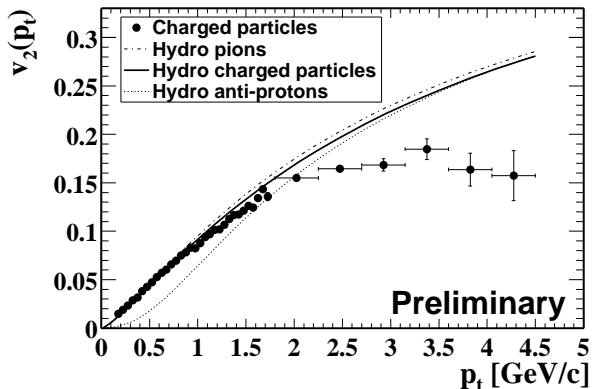


Figure 5.  $v_2(p_t)$  for charged particles and minimum-bias events, compared to hydro calculations [16].

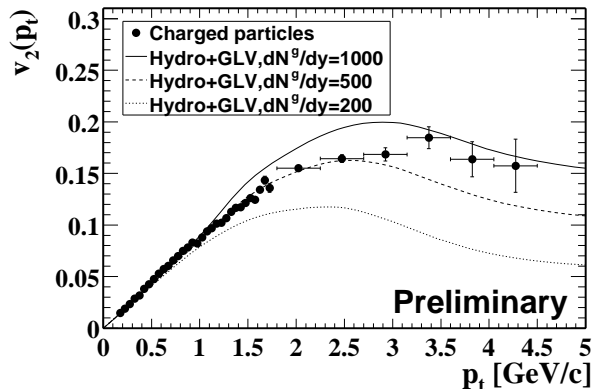


Figure 6.  $v_2(p_t)$  for charged particles and minimum-bias events, compared to pQCD calculations [17].

Figure 5 shows  $v_2(p_t)$  for charged particles, the error bars shown are only the statistical uncertainties. The systematic uncertainties are 13% up to 2 GeV/c, increasing to 20% at 4.5 GeV/c. The data show that up to  $p_t < 1.5$  GeV/c,  $v_2(p_t)$  increases almost linearly. This is consistent with a stronger “in-plane” expansion than the average radial expansion. In Fig. 5, a comparison is made with a full hydrodynamical model calculation [16], which describes the data up to  $p_t = 1.5$  GeV/c. Above  $p_t = 1.5$  GeV/c the  $v_2(p_t)$  starts to saturate and deviates from the hydro calculation. The  $v_2(p_t)$  above 2 GeV/c can be described by medium induced radiative energy loss of high  $p_t$  partons (jet quenching) [17]. However, one should note that the interplay between the “soft” physics and the onset of “hard” scattering without any energy loss could lead to a similar behavior. In the  $p_t$  range around 2–3 GeV/c both “soft” and “hard” physics are expected to contribute. Future measurements at  $p_t > 6$  GeV/c should be able to disentangle these interpretations. Figure 6 shows one of the calculations [17], which contains a phenomenological soft “hydrodynamic” component combined with a hard “pQCD” component incorporating energy loss. Comparing this calculation using different initial gluon densities with the data, shows a qualitative agreement up to the highest measured  $p_t$ .

### 3. Identified-particle differential elliptic flow

Hydrodynamics assumes complete local thermalization at the formation of the system followed by an evolution governed by an Equation Of State (EOS). Studies of the mass dependences of elliptic flow for particles with  $p_t < 1.5$  GeV/c provide important additional test of the hydrodynamical model.

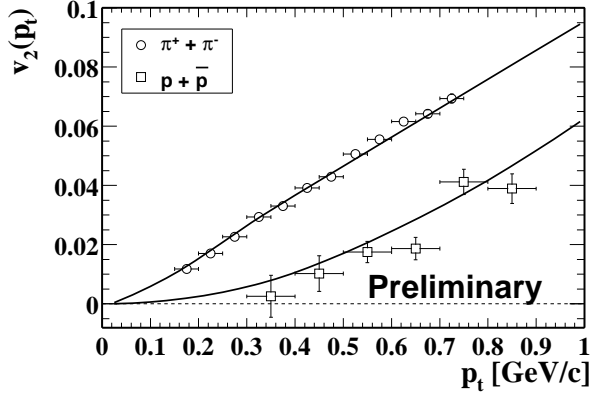


Figure 7.  $v_2(p_t)$  for pions and protons + anti-protons, the solid lines show the comparison with a full hydrodynamical model calculation [16].

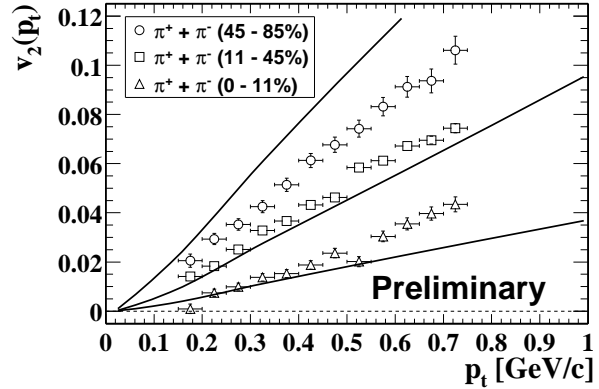


Figure 8.  $v_2(p_t)$  for pions in different centralities, the solid lines show the comparison with a full hydrodynamical model calculation [16].

The pions, protons and anti-protons, were selected according to specific energy loss ( $dE/dx$ ) in the TPC in the momentum range of 0.175 – 0.75 GeV/ $c$ , 0.5 – 0.9 GeV/ $c$  and 0.3 – 0.9 GeV/ $c$  respectively. The protons up to a momentum of 0.5 GeV/ $c$  were not used because of proton background from the beam pipe. The raw yields of the pions and protons + anti-protons were obtained from fitting the  $dE/dx$  distributions for each  $y, p_t$  bin with a multiple Gaussian fit and requiring greater than 90% purity.

In Fig. 7 the differential elliptic flow as a function of  $p_t$  for pions and protons + anti-protons for minimum-bias collisions is shown. The uncertainties shown are statistical only. Using the same assumption to estimate the systematic uncertainties as in section 2 and in addition assuming they are independent of  $p_t$ , the systematic uncertainty for minimum-bias data is 13%. The positive and negative identified particles, used in this analysis, have the same  $v_2(p_t)$  within statistical uncertainties. For  $v_2(p_t)$  the pions were integrated over  $|y| \leq 1.0$  and the protons + anti-protons over  $|y| \leq 0.5$ . The pions exhibit an almost linear dependence of  $v_2(p_t)$ , whereas the protons + anti-protons show a more quadratic behavior of  $v_2(p_t)$ . Such a behavior is the result of the interplay between the mean expansion velocity, the anisotropic component of the expansion velocity, and the thermal velocity of the particles. A similar effect was predicted for the case of directed flow [18] at AGS energies. The behavior is well described by a full hydrodynamical calculation [16]. This indicates that the minimum-bias data can be described using a hydrodynamic description with one set of parameters.

The differential elliptic flow  $v_2$  as a function of  $p_t$  is plotted for pions for three different centrality selections in Fig. 8. The open triangles, represent the most central 11% of the measured cross section<sup>2</sup>. The open squares correspond to 11 – 45% and the open circles

<sup>2</sup>The total measured cross section is estimated to correspond to about 80% to 90% of the geometric cross section, with losses mainly due to vertex finding inefficiencies for the low multiplicity events.

correspond to 45 – 85% of the measured cross section. The uncertainties on the points are statistical only. The systematic uncertainty is estimated to be 20% for the most central bin, 8% for the mid-central bin and 22% for the most peripheral bin. In Fig. 8 the lines show the comparison of the same hydrodynamical calculation for the different centralities. This comparison shows that the most central and the mid-peripheral data can be reasonably well described by this model. However, the most peripheral data clearly deviate from the hydrodynamical model predictions, indicating a lower degree of thermalization during the early stage of the collision for the most peripheral collisions.

#### 4. Conclusions

We have made the first measurement of identified particle elliptic flow at RHIC. The measured elliptic flow as a function of  $p_t$  and centrality differ significantly for particles of different masses. This mass dependence of  $v_2(p_t)$  is in close agreement with full hydrodynamic model calculations, suggesting that the system for central and mid-peripheral collisions is close to early local thermal equilibrium followed by hydrodynamic expansion. The observed deviation from hydro calculations at  $p_t > 1.5$  GeV/ $c$  indicates the transverse momentum region where thermal equilibrium is not reached. This region can be used to study parton energy loss in dense hadronic matter.

#### REFERENCES

1. For reviews and recent developments see these proceedings.
2. H. Sorge, Phys. Lett. **B402**, 251 (1997).
3. J.-Y. Ollitrault, Phys. Rev. D **46**, 229 (1992).
4. E877 Collaboration, J. Barrette *et al.*, Phys. Rev. C **55**, 1420 (1997).
5. E895 Collaboration, C. Pinkenburg *et al.*, Phys. Lett. **83**, 1295 (1999).
6. NA49 Collaboration, H. Appelshäuser *et al.*, Phys. Lett. **80**, 4136 (1998).
7. A.M. Poskanzer and S.A. Voloshin for the NA49 Collaboration, Nucl. Phys. **A661**, 341c (1999).
8. WA98 Collaboration, M.M. Aggarwal *et al.*, Phys. Lett. **B403**, 390 (1997); M.M. Aggarwal *et al.*, Nucl. Phys. **A638**, 459 (1998).
9. STAR Collaboration, K.H. Ackermann *et al.*, Phys. Lett. **86**, 402 (2001).
10. STAR Collaboration, K.H. Ackermann *et al.*, Nucl. Phys. **A661**, 681c (1999).
11. C. Adler *et al.*, preprint nucl-ex/0008005.
12. A.M. Poskanzer and S.A. Voloshin, Phys. Rev. C **58**, 1671 (1998).
13. N. Borghini, P.M. Dinh and J.-Y. Ollitrault, preprint nucl-th/0007063.
14. S.A. Voloshin and A.M. Poskanzer, Phys. Lett. **B474**, 27 (2000).
15. M. Gyulassy and X.N. Wang, Comp. Phys. Comm. **83**, 307 (1994); Phys. Rev. **D44**, 3501 (1991).
16. P. Huovinen *et al.*, Phys. Lett. **B503**, 58 (2001); private communication.
17. M. Gyulassy, I. Vitev and X.N. Wang, Phys. Rev. Lett. **86**, 2537 (2001).
18. S. Voloshin, Phys. Rev. C **55**, 1630 (1997).